RIS-AIDED MMWAVE BEAM-FORMING FOR TWO-WAY COMMUNICATIONS OF MULTIPLE PAIRS

Nariman Torkzaban[1], Mohammad A. (Amir) Khojastepour[2], Mohammad Farajzadeh-Tehrani[3], John S. Baras[4]

[1]Institute for Systems Research (ISR) and the Department of Electrical and Computer Engineering, University of Maryland, College Park, MD, 20740 USA e-mail: (narimant@umd.edu), [2]NEC Laboratories, America Inc., Princeton, NJ, 08540 USA e-mail: (amir@nec-labs.com), [3]Mathematics Department, University of Iowa, Iowa City, IA, 52242 USA e-mail: (mohammad-tehrani@uiowa.edu), [4]Institute for Systems Research (ISR) and the Department of Electrical and Computer Engineering, University of Maryland, College Park, MD, 20740 USA e-mail: (baras@umd.edu)

NOTE: Corresponding author: Mohammad A. (Amir) Khojastepour, amir@nec-labs.com

Abstract – *Millimeter-wave (mmWave) communications is a key enabler towards realizing enhanced Mobile Broadband (eMBB) as a key promise of 5G and beyond, due to the abundance of bandwidth available at mmWave bands. An mmWave coverage map consists of blind spots due to shadowing and fading especially in dense urban environments. Beam-forming employing massive MIMO is primarily used to address high attenuation in the mmWave channel. Due to their ability in manipulating the impinging electromagnetic waves in an energy-efficient fashion, Reconfigurable Intelligent Surfaces (RISs) are considered a great match to complement the massive MIMO systems in realizing the beam-forming task and therefore effectively filling in the mmWave coverage gap. In this paper, we propose a novel RIS architecture, namely RIS-UPA where the RIS elements are arranged in a Uniform Planar Array (UPA). We show how RIS-UPA can be used in an RIS-aided MIMO system to fill the coverage gap in mmWave by forming beams of a custom footprint, with optimized main lobe gain, minimum leakage, and fairly sharp edges. Further, we propose a configuration for RIS-UPA that can support multiple two-way communication pairs, simultaneously. We theoretically obtain closed-form low-complexity solutions for our design and validate our theoretical findings by extensive numerical experiments.*

Keywords – Blind-spot coverage, multi-beamforming, reconfigurable intelligent surface, RIS-aided MIMO, uniform planar array

1. INTRODUCTION

The next generation of wireless communication systems aims to address the ever-increasing demand for high throughput, low latency, better quality of service, and ubiquitous coverage. The abundance of bandwidth available at the mmWave frequency range, i.e., $[20, 100]$ GHz, is considered as a key enabler towards the realization of the promises of next generation wireless communication systems. However, communication in mmWave suffers from high path-loss and poor scattering and diffraction. Therefore, mmWave signals are vulnerable to blockages, especially in urban areas. In fact, since the channel in mmWave is mostly line-of-sight (LoS), i.e., a strong LoS path and very few and much weaker secondary components, the mmWave coverage map includes *blind spots* as a result of shadowing and blockage. Beam-forming employing massive MIMO is primarily used to address the high attenuation in the mmWave channel. In addition to beamforming, relaying can potentially be designed to generate constructive superposition and enhance the received signals at the receiving nodes. Equipping MIMO communication systems by Reconfigurable Intelligent Surfaces (RISs) may extend the capacity of mmWave by covering the blind spots and providing diversity reception at the receiving nodes.

RIS [1][2][3] is denoted as a potential enabling technology for realizing 6G-and-beyond [4][5] due to its great potential for manipulating the impinging electromagnetic waves and artificially shaping the wireless propagation environment in a cost-effective and energy-efficient manner. The wireless propagation environment in current communication systems is considered to be uncontrollable and stochastic, and therefore, the existing wireless system design technologies and principles (e.g., mmWave communication systems, massive MIMO, etc.) are traditionally developed on a reactive basis to adapt to this stochastic behavior. An RIS typically consists of a large number of low-cost and passive reflecting elements arranged in planar artificial metasurfaces. Each RIS cell is capable of manipulating the phase and possibly the amplitude of incident electromagnetic waves in response to real-time external signals provided by a smart controller. The programmability of the RIS enables them to flexibly modulate RF signals without the need to use any mixers, analog phase-shifters, analog-to-digital/ digital-to-analog converter, etc. [6][7]. This not only drives the RIS hardware cost and energy consumption down, but also allows for the design of RF chain-free wireless transceivers [8][9]. Therefore, either as active transceivers or passive reflectors, RIS may be a promising solution to revolutionize the design of the physical layer in next-generation wireless communication systems.

1.1 Related work

RISs have attracted a lot of attention both from industry and academia, over the past several years. The efforts towards realizing the prospects of achieving RIS-aided wireless communications initially started with theoretical developments based on mathematical models. More recently, real-world trials with prototyping and field experiments have been pursued more seriously than before in the literature. Several funding agencies have heavily invested in theoretical development, designing, prototyping, and testing the intelligent metamaterial surfaces. Since 2012, the National Science Foundation (NSF) in the US, and the European Commission, Horizon 2020, have spent millions of dollars in projects tackling different aspects of the reflective metasurfaces and integrating the RIS with next generation networks [10].

With respect to experimental trials, extensive efforts have been made. The Japanese network operator NTT DoCoMo in collaboration with its partners has repeated a few successful trials over the past couple of years, demonstrating how their designed transparent dynamic metasurface can improve the power of the radio signal at 28 GHz [11]. In [12], the authors have proposed a prototype for RIS-enabled wireless communications with an RIS consisting of 1100 elements operating at 5.8 GHz. They show their passive reflect-array design provides significant gain improvement in point-to-point wireless communications through indoor and outdoor field trials. Another prototype is proposed in [13] for modulating the incident waves based on single-carrier Quadrature Phase Shift Keying (QPSK) to design RIS-based transceivers achieving a 2.048 Mbps data rate for video-streaming. The prototype in [8] achieves an RIS-based RF-chain free transceiver.

RISs are promising to be deployed in a wide range of communications scenarios, such as high throughput MIMO communications [9][14], ad-hoc networks, e.g., UAV communications [15][16], physical layer security [17], etc. In radar, deployment of RISs with judicious design of phase shifts has shown improvement in estimation of the radar cross-section [18] and moving target [19]. Apart from the work focusing on theoretical performance analysis of RIS-enabled systems [20][21], considerable amount of work has been dedicated to optimizing such an integration, mostly focusing on the phase optimization of RIS elements [22][23][24] to achieve various goals such as maximum received signal strength, maximum spectral efficiency, etc. For more information on the challenges and opportunities associated with RIS, we refer the interested readers to [25][26] and the references therein.

In this paper, we present an RIS-aided architecture to facilitate two-way communications. Most of the prior art in RIS-aided two-way communications, focuses on single-beam communications [27][28]. However, in this paper we propose the idea of RIS-aided multi-beamforming. The idea of RIS-aided multi-beamforming, i. e., beamforming with multiple disjoint lobes, was first introduced in [29], where the authors aimed at covering the mmWave blind spots by designing sharp beams covering various ranges of solid angle. The codebook design problem for such beam-forming was addressed in [30]. In [31], the authors employ dual beam-forming for short range target monitoring.

1.2 Main contributions

In this paper, we consider a communication scenario between a transmitter, e.g., the Base Station (BS), and terrestrial end users through a passive RIS that reflects the received signal from the transmitter towards the users. Hence, the users that are otherwise in blind spots of network coverage become capable of communicating with the base station through the RIS that is serving as a passive reflector (passive relay) maintaining communication links between the BS and the users. Given the geospatial variance among the locations of the end users served by the same wireless system, the RIS may have to simultaneously accommodate users that lie in different angular intervals that are widely separated with a satisfactory Quality of Service (QoS). In what we refer to as *multi-beamforming*, we particularly address the design of beams consisting of multiple disjoint lobes in order to cover different blind spots using sharp, high gain, and effective beam patterns. In the following, we summarize the main contributions of this paper:

- **[RIS-UPA to UPA Transformation]** We present simple yet important properties of RIS with UPA structure (RIS-UPA) when used as a beam-former in Section 3. As a consequence, we present a transformation between the beam-former design problem in UPA and RIS-UPA which allows us to directly borrow the design for UPA beam-forming and by the means of a transformation use it for RIS-UPA beam-forming.
- **[Multi-beamforming]** We present a new beamforming design technique termed as *multi-beamforming* aiming to design beams with multiple disjoint lobes. The multi-beamforming design inherently depends on the solid angle (say Ω_1 in Fig. 1) at which the incident wave activates the RIS elements. The proposed beam-forming design easily adapts to changes in Ω_1 and we provide a visualization as to how the beam would change in response to change in Ω_1.
- **[Custom footprint]** The proposed method has the flexibility to design a beam with a custom footprint. The beam footprint may be defined as the cross-section of the beam lobes with the sphere (say at beam gains within the half-power (3dB) point and maximum gain).
- **[Compound beams]** We design the parameters of the RIS to achieve multiple disjoint beams covering various ranges of a solid angle. The designed beams are fairly sharp, have almost uniform gain in the desired Angular Coverage Interval (ACI), and have negligible power transmitted outside the ACI.

- **[Complexity]** Thanks to the derived analytical closed form solutions for the multi-beamforming design, the proposed solution bears very low computational complexity even for an RIS with massive array sizes.
- **[Multilink]** We also provide RIS beam-forming design in multilink scenarios where different pairs of transmitters and receivers are communicating simultaneously with the help of the same RIS. Moreover, we establish a connection between multilink beam-forming and multi-beamforming.
- **[Evaluation]** Through numerical evaluation we show that by using a passive RIS, multi-beamforming can simultaneously cover multiple ACIs. Moreover, multi-beamforming provides tens of dB power boost w.r.t. the single-beam RIS design.

1.3 Notations

Throughout this paper, $\mathbb{C}$, $\mathbb{R}$, and $\mathbb{Z}$ denote the set of complex, real, and integer numbers, respectively, $\mathcal{CN}(m, \sigma^2)$ denotes the circular symmetric complex normal distribution with mean m and variance σ^2, $[a, b]$ is the closed interval between a and b, $[m]$ is the set of m positive integers less than or equal to m, $[(m, n)]$ is the set of all $m \times n$ integer pairs with the first element less than m and the second element less than n, $\mathbf{1}_{a,b}$ is the $a \times b$ all ones matrix, $\mathbf{I}_N$ is the $N \times N$ identity matrix, $1_{[a,b)}$ is the indicator function, $\| \cdot \|$ is the 2-norm, $\| \cdot \|_\infty$ is the infinity-norm, $| \cdot |$ may denote cardinality if applied to a set and 1-norm if applied to a vector, $\odot$ is the Hadamard product, $\otimes$ is the Kronecker product, the operator diag$\{.\}$ when applied to a square matrix takes the vector of its diagonal elements, and when applied to a vector of elements, forms a diagonal matrix of that vector, $\mathbf{A}^H$, and $\mathbf{A}_{a,b}$ denote conjugate transpose, and $(a, b)^{th}$ entry of $\mathbf{A}$ respectively. We have summarized the list of variables and parameters frequently used in the paper in Table 1.

1.4 Organization

The remainder of the paper is organized as follows. Section 2 develops the system model by describing the channel model and the RIS configuration. In Section 3 we present a few fundamental properties of the gain provided by the RIS-aided system that are central to our design in the subsequent sections. In Section 4 we describe the multi-pair two-way communications problem and illustrate how it can be posed as a MIMO beam-forming problem. Then we present the corresponding problem formulation. In Section 5 we propose our approach for solving the RIS-enabled multi-pair two-way communications problem resulting in a closed-form expression for the con iguration of the RIS. Section 6 presents the evaluation results for our numerical experiments verifying the effectiveness of our solution, and inally, we conclude in Section 7.

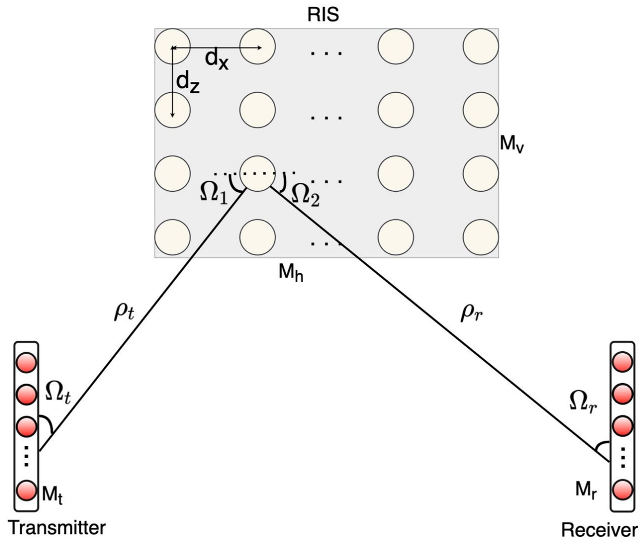

Fig. 1 – System model

2. SYSTEM MODEL

2.1 Channel model

Consider a communication system consisting of a multi-antenna BS with M_t antenna elements as a transmitter and a multi-antenna receiver with M_r antenna elements. The MIMO system is aided by a multi-element RIS consisting of M elements arranged in an $M_h \times M_v$ grid in the form of a UPA as shown in Fig. 1, where M_h and M_v are the number of elements in the horizontal and vertical directions, respectively. The received signal $\mathbf{y} \in \mathbb{C}^{M_r}$ as a function of the transmitted signal $\mathbf{x} \in \mathbb{C}^{M_t}$ can be written as,

$$\mathbf{y} = (\mathbf{H}_r \mathbf{\Theta} \mathbf{H}_t)\mathbf{x} + \mathbf{z} \tag{1}$$

where $\mathbf{z}$ is the noise vector, where each element of $\mathbf{z}$ is drawn from a complex Gaussian distribution $\mathcal{CN}\left(0, \sigma_n^2\right)$, $\mathbf{H}_t \in \mathbb{C}^{M \times M_t}$ and $\mathbf{H}_r \in \mathbb{C}^{M_r \times M}$ are the channel matrices between each party and the RIS. We assume that the RIS consists of elements for which both the phase θ_m and the gain β_m (in form of the attenuation of the reflected signal) of each element, say m, may be controlled and $\mathbf{\Theta} \in \mathbb{C}^{M \times M}$ is a diagonal matrix where the element (m, m) denotes the coefficient $\beta_m e^{j\theta_m}$ of the m^{th} element of the RIS. Assuming a LoS channel model both between the transmitter and the RIS and between the RIS and the receiver and using the directivity vectors at the transmitter, the RIS, and the receiver, the effective channel matrices can be written as,

$$\mathbf{H}_r = \mathbf{a}_{M_r}(\Omega_r)\rho_r \mathbf{a}_M^H(\Omega_2) \tag{2}$$

$$\mathbf{H}_t = \mathbf{a}_M(\Omega_1)\rho_t \mathbf{a}_{M_t}^H(\Omega_t) \tag{3}$$

Table 1 – Frequently-used parameters and variables

Variables	Description
$\mathbf{\Theta}$	The decision variables representing the coefficients of RIS elements manipulating the impinging electromagnetic waves
$\boldsymbol{\lambda}$	The decision variables representing the overall impact of the RIS when excited from an incident solid AoA of Ω_1
$\mathbf{c}$	The normalized version of λ, or equivalently, the normalized beam-forming vector corresponding to a Uniform Planar Array (UPA) of antennas
$\mathbf{g}$	Equal-gain vector that has to be optimally chosen when deciding the optimal configuration **c**.
$\Gamma(\Omega_1, \Theta, \Omega)$	The gain of an RIS configured by $\mathbf{\Theta}$ at AoD Ω when excited from an incident angle Ω_1.
$G(\xi, \zeta, \boldsymbol{\lambda})$	The beam-forming gain of a UPA of antennas configured by $\boldsymbol{\lambda}$ at AoD $\psi = [\xi, \zeta]$
η	The design parameter embedded in **g** determining the quality of the beams formed by the multi-beamforming approach.
Parameters	Description
$\mathbf{H}_t$	The effective channel matrix from the transmitter to the RIS
$\mathbf{H}_r$	The effective channel matrix from the RIS to the receiver
$\mathbf{a}_M(\Omega)$	The array response vector of an array of M antennas or an RIS consisting of M elements at the solid angle Ω
ρ_t	The gain of the Line-of-Sight (LoS) path from the transmitter to the RIS
ρ_r	The gain of the Line-of-Sight (LoS) path from the RIS to the receiver
Ω_t	The Angle of Departure (AoD) from the transmitter towards the RIS
Ω_r	The Angle of Arrival (AoA) from the RIS at the receiver
Ω_1	The Angle of Arrival (AoA) from the transmitter at the RIS
Ω_2	The Angle of Departure (AoD) from the RIS towards the receiver
$\tau(\Omega)$	The operator τ maps the solid angle $\Omega = [\phi, \theta]$ to $\psi = [\xi, \zeta] = \tau(\Omega)$
$\mathbf{d}_M(\psi)$	The directivity vector of an array of antennas at direction ψ
$\mathcal{B}$	The total angular range under study in the Ω domain
$\mathcal{B}^\psi$	The total angular range under study in the ψ domain
$\mathcal{D}_n$	The n-th receive zone in the n-th communication pair
$\mathcal{A}_n$	The minimal index set of the particles covering the n-th receive zone $\mathcal{D}_n$
$\mathcal{B}^\psi_{p,q}$	The area covered by the (p, q)-th particle in the ψ-domain
$\mathbf{e}_{p,q}$	The vector with a 1 in the (p, q)-th entry out of $[(Q_v, Q_h)]$ ones and zero everywhere else

where $\mathbf{a}_M(\Omega)$ is the array response vector of an RIS with elements in a UPA structure (RIS-UPA), Ω_t and Ω_2 are the solid Angles of Departure (AoD) of the transmitted beams from the transmitter and the RIS and Ω_1 and Ω_r are the solid Angles of Arrival (AoA) of the received beams at the RIS and the receiver, respectively.

The gains of the LoS paths from the transmitter to the RIS and from the RIS to the receiver are denoted by ρ_t and ρ_r, respectively. Note that an arbitrary solid angle Ω specifies a pair of elevation and azimuth angles (ϕ, θ). Therefore, in the above definitions we set $\Omega_a = [\phi_a, \theta_a]$, $a \in \{1, 2, t, r\}$. Further, assuming no pairing between the RIS elements, $\mathbf{\Theta}$ will be a diagonal matrix specified as

$$\mathbf{\Theta} = \text{diag}\{[\beta_1 e^{j\theta_1}, \dots, \beta_M e^{j\theta_M}]\} \tag{4}$$

where $\beta_i \in [0, 1]$ and $\theta_i \in [0, 2\pi]$. Using equations *(1)-(3)*, the contribution of the RIS to the channel matrix when excited from incident angle Ω_1 for a receiver at a given solid angle solid angle Ω is given by

$$\Gamma(\Omega_1, \mathbf{\Theta}, \Omega) = \mathbf{a}_M^H(\Omega)\mathbf{\Theta}\mathbf{a}_M(\Omega_1) = \mathbf{a}_M^H(\Omega)\boldsymbol{\lambda} \tag{5}$$

where we define $\boldsymbol{\lambda} = \mathbf{\Theta}\mathbf{a}_M(\Omega_1)$, $\boldsymbol{\lambda} \in \mathbb{C}^M$.

2.2 RIS model

Consider an RIS consisting of $M_v \times M_h$ antenna elements forming a UPA structure that is placed at the x-z plane, where $M \doteq M_v M_h$ and the z-axis corresponds to the horizon. Let d_z, and d_x denote the distance between the antenna elements in the z and x axis, respectively. Throughout this paper, we assume that the transmitter and the receiver are within the far field of the RIS. As opposed to the near-field regime, the diversity gain distribution in the far field does not depend on the distance between the transmitter and the RIS[32]. RIS-enabled communications in the near field requires a thoroughly different design. For an example of such a specification, please refer to [33]. The array response vector of an RIS-UPA can be found in a similar way to that of a UPA. At a solid angle $\Omega = [\phi, \theta]$, we have

$$\mathbf{a}_M(\Omega) = \left[1, e^{j\frac{2\pi}{\lambda}\mathbf{r}_\Omega \mathbf{r}_1}, \dots, e^{j\frac{2\pi}{\lambda}\mathbf{r}_\Omega \mathbf{r}_{M-1}}\right]^T \in \mathbb{C}^M \tag{6}$$

where we define $\mathbf{r}_\Omega = [\cos\phi\cos\theta, \cos\phi\sin\theta, \sin\phi]$, and $\mathbf{r}_m = (m_h d_x, 0, m_v d_z)$ to respectively denote the direction corresponding to the solid angle Ω, and the location of the m-th RIS element corresponding to the antenna placed at the position (m_v, m_h) with $m = m_v M_h + m_h$.
Further, we define a transformation of variables as follows. For a solid angle $\Omega = [\phi, \theta]$, define $\psi = [\xi, \zeta]$

$$\xi = \frac{2\pi d_z}{\lambda}\sin\phi, \quad \zeta = \frac{2\pi d_x}{\lambda}\sin\theta\cos\phi \tag{7}$$

Introducing the new variables into equation *(6)*, it is straightforward to write,

$$\mathbf{a}_M(\Omega) = \mathbf{d}_M(\psi) = \mathbf{d}_{M_v}(\xi) \otimes \mathbf{d}_{M_h}(\zeta) \in \mathbb{C}^M \tag{8}$$

where $\mathbf{d}_M$ denotes the directivity vector of the RIS, and the directivity vectors $\mathbf{d}_{M_a}$, $a \in \{v, h\}$ are defined as follows.

$$\mathbf{d}_{M_v}(\xi) = \left[1, e^{j\xi} \cdots e^{j(M_v-1)\xi}\right]^T \in \mathbb{C}^{M_v}$$
$$\mathbf{d}_{M_h}(\zeta) = \left[1, e^{j\zeta} \cdots e^{j(M_h-1)\zeta}\right]^T \in \mathbb{C}^{M_h} \tag{9}$$

where $\psi_v = \xi$, and $\psi_h = \zeta$. Finally, let $\mathcal{B}$ be the angular range for Ω under our interest defined as follows,

$$\mathcal{B} = \left[-\phi^{\mathrm{B}}, \phi^{\mathrm{B}}\right) \times \left[-\theta^{\mathrm{B}}, \theta^{\mathrm{B}}\right) \tag{10}$$

Accordingly, let $\mathcal{B}^{\psi}$ be the angular range under interest in the (ξ, ζ) domain given by

$$\mathcal{B}^{\psi} = \left[-\xi^{\mathrm{B}}, \xi^{\mathrm{B}}\right) \times \left[-\zeta^{\mathrm{B}}, \zeta^{\mathrm{B}}\right) \tag{11}$$

In this paper, we set $d_x = d_z = \frac{\lambda}{2}$, $\phi^{\mathrm{B}} = \frac{\pi}{4}$, and $\theta^{\mathrm{B}} = \frac{\pi}{2}$, hence $\xi \in [-\pi\frac{\sqrt{2}}{2}, \pi\frac{\sqrt{2}}{2})$, and $\zeta \in [-\pi, \pi)$. To formalize the variable transformation introduced in *(7)*, we define the transformation operator $\tau : \mathcal{B} \longrightarrow \mathcal{B}^{\psi}$ as $\tau([\phi, \theta]) = [\xi, \zeta]$.

3. GENERAL PROPERTIES OF RIS AS BEAM-FORMER

For a RIS-UPA excited by an emission from solid angle Ω_1, we can write for the reference gain at any direction Ω,

$$\begin{aligned} |\Gamma(\Omega_1, \Theta, \Omega)| &= |\mathbf{a}_M^H(\Omega)\Theta\mathbf{a}_M(\Omega_1)| \\ &= \left|\sum_{m=0}^{M-1} \theta_{m,m} e^{-j(m_v\xi + m_h\zeta)} e^{j(m_v\xi_1 + m_h\zeta_1)}\right| \\ &= \left|\sum_{m=0}^{M-1} \theta_{m,m} e^{j(\tau(\Omega_1) - \tau(\Omega))\mathbf{m}}\right| \end{aligned} \tag{12}$$

where we define $\mathbf{m} = [m_v, m_h]^T$. In the following we present three fundamental facts together with their interpretation, that are useful for our subsequent developments in the next sections. The proofs for all these facts is straightforward and can be achieved by basic calculus. First of all, from the identity,

$$|\Gamma(\Omega_1, \mathrm{diag}\{\mathbf{a}_M^H(\Omega_1)\Theta\}, \Omega)| = |\Gamma(0, \Theta, \Omega)| \tag{13}$$

we note that the gain of a UPA with beam-forming matrix Θ at any solid angle Ω is equal to that of a RIS-UPA excited from an AOA Ω_1 with parameter matrix $\mathrm{diag}(\mathbf{d}_M^H(\psi_1)\Theta))$. Second, for any solid angle Ω_2, with $\tau(\Omega_2) = \psi_2$, it holds that,

$$|\Gamma(\Omega_1, \Theta, \Omega)| = |\Gamma(\Omega_1, \mathrm{diag}\{\mathbf{a}_M^H(\Omega_2)\Theta\}, \Omega')| \tag{14}$$

where $\tau(\Omega') = \tau(\Omega) - \tau(\Omega_2)$. The last identity implies that for two RIS-UPAs with parameter matrices Θ and $\mathrm{diag}\{\mathbf{d}_M^H(\psi_2)\Theta\}$ that are excited from the same AoA Ω_1, the gain patterns are just a rotation of each other such that the gain at direction Ω for the first one is equal to the gain at the direction of Ω' for the second one, where Ω' is as denoted above. The same holds for a UPA by setting $\Omega_1 = 0$., i.e., the gain pattern of two UPAs with parameters Θ and $\mathrm{diag}\{\mathbf{d}_M^H(\psi_2)\Theta\}$ are related by a rotation of each other such that the gain at direction Ω for the first one is equal to the gain at the direction of Ω' for the second one. Finally, it is straightforward to show,

$$|\Gamma(\Omega_1, \Theta, \Omega)| = |\Gamma(\Omega_2, \Theta, \Omega^{''})| \tag{15}$$

where $\tau(\Omega'') = \tau(\Omega) + \tau(\Omega_2) - \tau(\Omega_1)$. By virtue of the last identity, we note that for two RIS-UPAs with the same parameters Θ that are excited from two different AoA Ω_1 and Ω_2 the gain patterns are just a rotation of each other such that the gain at direction Ω for the first one is equal to the gain at the direction of Ω'' for the second one, where Ω'' is obtained as above. As we will see in Section 4.2, we use this property to transform a Multi-Transmitter Multi-Receiver (MTMR) communication system to a Single-Transmitter Multi-Receiver (STMR) system. Consequently, it will enable us to design a single RIS to accommodate communications between multiple disjoint pairs, possibly with large angular separations.

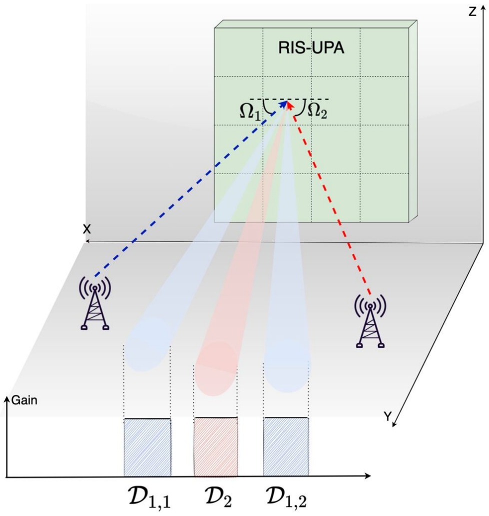

Fig. 2 – RIS-enabled two-way communications

Please note that if a user is located at the solid angle Ω with respect to the RIS, then the AoA of the incident wave at the RIS when the user is transmitting is defined as $\Omega = [\phi, \theta]$. However, due to the change in the direction of the beam, the reflected beam from an RIS towards the user is directed at angle $\Omega^r = [-\phi, \theta + \pi]$. Hence, from *(7)* and by the definition of the operator τ, we have $\tau(\Omega^r) = -\tau(\Omega)$. From *(12)*, for an RIS which is excited from an incident angle with AoA of $\Omega_1 = [\phi_1, \theta_1]$ reflects the signal with AoD of $\Omega_2 = [\phi_2, \theta_2]$, we have

$$|\Gamma(\Omega_1, \Theta, \Omega_2^r)| = |\Gamma(\Omega_2, \Theta, \Omega_1^r)| \tag{16}$$

where $\Omega_1^r = [-\phi_1, \theta_1 + \pi]$ and $\Omega_2 = [-\phi_2, \theta_2 + \pi]$. which means that the RIS has the same gain at the AoD of Ω_1^r when it is excited from the incident angle with AoA of Ω_2^r. This is trivially equivalent to the channel reciprocity property which indicates the possibility of two-way communications between each pair.

4. PROBLEM FORMULATION

In this section, we show how RIS can be used to simultaneously facilitate two-way communications between multiple pairs. We will first present the description of the problem and explain our approach. We then proceed with the formulation of the problem and propose our solution.

4.1 Problem description

We study the RIS design problem for RIS-enabled two-way communications where multiple communications pairs are involved. Each pair realizes a MIMO system consisting of a multi-antenna transmitter (e.g. multi-antenna BS), and a possibly multi-antenna receiver (e.g. multi-antenna mobile user). We assume there is no LoS channel between the pairs and the mmWave channel is assisted by an RIS with elements that are arranged according to a UPA structure.

Formally, we consider N communications pairs specified by $(\Omega_n, \mathcal{D}_n)$, $n = 1, \ldots, N$. The n-th transmitter is emitting at the RIS with an AoA of Ω_n, and the n-th receiver may reside within the receive zone $\mathcal{D}_n$, i.e., $\mathcal{D}_n$ represents the range of AoDs from the RIS that may cover the n-th receiver. For the n-th receive zone, we denote each continuous range of such AoDs by an Angular Coverage Interval (ACI). We note that each receive zone may comprise of one or more ACIs. Fig. 2 depicts an example of such a setup for $N = 2$ pairs, where receive zone $\mathcal{D}_1 = \mathcal{D}_{1,1} \cup \mathcal{D}_{1,2}$ consists of two ACIs. As far as the n-th communications pair is concerned, the *ideal* RIS must be configured in such a way that when excited from solid angle Ω_n it covers the receive zone $\mathcal{D}_n$ uniformly, with high and sharp gains, while leaving minimal gain leakage to other intervals. In RIS-aided MTMR two-way communications, we aim to design the RIS such that all pairs are satisfied simultaneously with a high QoS. The simplest instance of the above problem is when $N = 1$, i.e. when there is only one pair. We denote this instance by STMR.

Further, we note that (i) the boundaries of the ACIs are determined based on the potential locations of the receivers, and, (ii) we wish to consider the ACIs of minimal size to avoid sacrificing the gain. Therefore, the footprint of the receive zones on spherical coordinates may become of arbitrary shape. This may introduce additional complexity into the RIS design problem. To resolve this issue, let us uniformly divide $\mathcal{B}^{\psi}$ into $Q = Q_v Q_h$ subregions, where Q_v and Q_h determine the division resolution in the vertical and horizontal directions, respectively. We denote each such subregion by a *particle* $\mathcal{B}^{\psi}_{p,q}$ that is specified as,

$$\mathcal{B}^{\psi}_{p,q} = \nu^p_v \times \nu^q_h, \quad p \in [Q_v], q \in [Q_h] \tag{17}$$

where $\nu^p_v = [\xi^{p-1}, \xi^p]$, and $\nu^q_h = [\zeta^{q-1}, \zeta^q]$ defining,

$$\xi^p = -\xi^{\mathrm{B}} + p\delta_v, \quad \zeta^q = -\zeta^{\mathrm{B}} + q\delta_h \tag{18}$$

with $\delta_v = \frac{2\xi^{\mathrm{B}}}{Q_v}$, and $\delta_h = \frac{2\zeta^{\mathrm{B}}}{Q_h}$. Further, define for all (p, q) pairs the notation $\delta_{p,q} = \delta_v \delta_h$. We wish to cover each receive zone $\mathcal{D}_n$ in the RIS-enabled MTMR problem with the smallest set of particles, i.e., $\mathcal{D}_n \sim \bigcup_{(p,q)\in\mathcal{A}_n} \mathcal{B}^{\psi}_{p,q}$, with $\mathcal{A}_n$ being the smallest set of index pairs (p, q) that beams $\mathcal{B}^{\psi}_{p,q}$ collectively cover $\mathcal{D}_n$. The union of $\mathcal{B}^{\psi}_{p,q}$ is in fact approximating the shape of the desired receive zone $\mathcal{D}_n$, where the resolution of the approximation is set by the pair (Q_v, Q_h). By using larger values of Q_v, and Q_h, one can opt for finer particles and boost the quality of the approximation at the expense of solving a larger optimization problem. Explicitly, we have

$$\mathcal{A}_n = \arg\min_{\{\hat{\mathcal{A}} | \mathcal{D}_n \subseteq \bigcup_{(p,q)\in\mathcal{A}} \mathcal{B}_{p,q}\}} |\hat{\mathcal{A}}|, \quad n \in [N]. \tag{19}$$

Further define $\mathcal{A} = \bigcup_{n=1}^{N} \mathcal{A}_n$. Next, we will show how every instance of MTMR can be cast as an STMR problem. Then we pose the two-way communications problem in the STMR case, as a composite beam-forming problem under the UPA antenna structure. We then propose a low-complexity closed-form for the optimal solution to the last problem.

4.2 Transformation between MTMR and STMR

Consider N communications pairs $(\Omega_n, \mathcal{D}_n)$, $n = 1, \ldots, N$, where Ω_n is the AoA of the n-th transmitter to the RIS-UPA plane, and $\mathcal{D}_n$ denotes the n-th receive zone. For an arbitrary RIS-UPA configuration $\hat{\Theta}$, and for any communications pair, by equation *(15)*, we get

$$|\Gamma(\Omega_n, \hat{\Theta}, \Omega)| = |\Gamma(\Omega_1, \hat{\Theta}, \tilde{\Omega})|, \quad \forall n \in [N]. \tag{20}$$

where $\tau(\tilde{\Omega}) = \tau(\Omega) + \tau(\Omega_1) - \tau(\Omega_n)$. This would mean under the ψ-domain that if $\hat{\Theta}$ is optimized to cover the angular interval $\mathcal{D}_n$, when excited from an AoA of Ω_n, same configuration when excited from an AoA of Ω_1 will cover the angular interval $\tilde{\mathcal{D}}_n$ that is a shifted version of $\mathcal{D}_n$, by $\tau(\Omega_1) - \tau(\Omega_n)$. Therefore, instead of solving the RIS-enabled MTMR two-way communications problem under transmission pairs $(\Omega_n, \mathcal{D}_n)$, $n \in [N]$, we propose to solve an RIS-enabled STMR two-way communications problem with the transmission pair $(\Omega_1, \tilde{\mathcal{D}})$, where $\tilde{\mathcal{D}} = \bigcup_{n=1}^{N} \mathcal{D}_n$. Let $\tilde{\boldsymbol{\Theta}}^*$ be the optimal configuration of the RIS-UPA derived for solving the STMR problem. Then a straightforward use of equation *(15)* in the reverse order for each n, will verify that $\boldsymbol{\Theta} = \tilde{\boldsymbol{\Theta}}^*$ is the optimal RIS-UPA configuration for the MTMR case. An example of the above transformation is illustrated for $N = 2$ in Fig. 3. Fig 3(a) depicts the receive zones $\mathcal{D}_n$, $n = 1, 2$, over the ψ-domain. Each receive zone only consists of one ACI and the particle resolution is set to $(Q_v, Q_h) = (24, 24)$. Using equation *(15)*, the receive zone $\mathcal{D}_2$ will get shifted by $\tau(\Omega_1) - \tau(\Omega_2)$ to form $\mathcal{D}'_2$. Fig. 3(b) depicts this transition. As the result of this transformation Fig. 3(c) plots the corresponding STMR receive zone $\tilde{\mathcal{D}} = \mathcal{D}_1 \cup \mathcal{D}'_2$ that is comprised of two ACIs.

4.3 Relationship between RIS-UPA and UPA-antenna beam-forming

RIS-UPA refers to an RIS with UPA structure while UPA-antenna refers to a regular multi-element antenna array where the elements are arranged in the same UPA structure. In this section, we clarify the relation between the

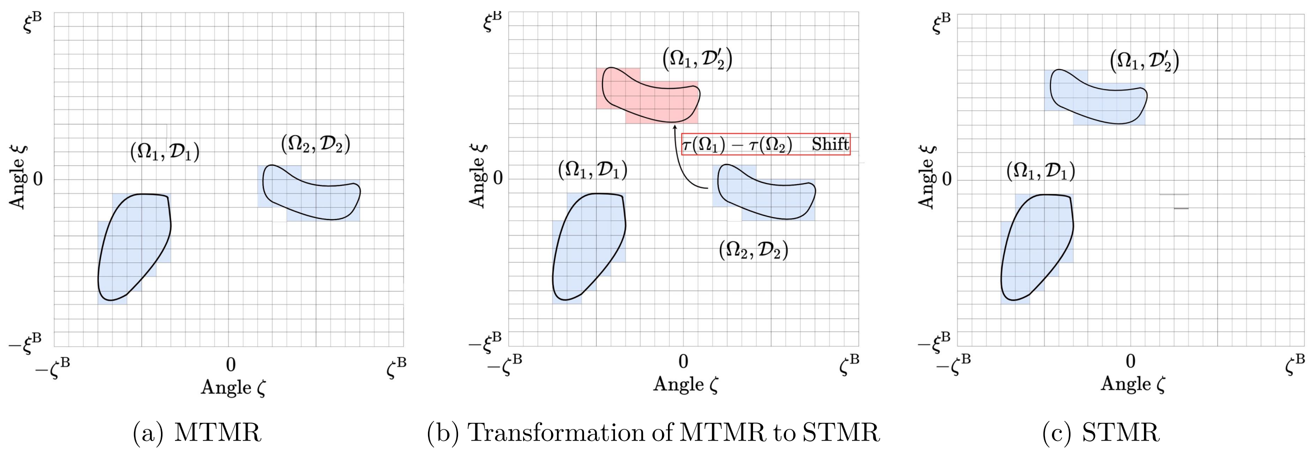

Fig. 3 – Transforming two-way MTMR to STMR communications

beam-forming gain of an RIS-UPA and its UPA-antenna counterpart.

We start by explicitly writing $\boldsymbol{\lambda}$ in equation *(5)* in terms of its elements as follows

$$\boldsymbol{\lambda} = [\lambda_{0,0}, \ldots, \lambda_{0,M_h-1}, \lambda_{1,0}, \ldots, \lambda_{M_v-1,M_h-1}] \quad (21)$$

where λ_{m_v,m_h} corresponds to the element located at position (m_v, m_h) in the UPA grid. Using the expressions *(6)*-*(9)*, for an RIS-UPA that is excited from an incident angle Ω_1, we have

$$\begin{aligned}\lambda_{m_v,m_h} &= \beta_{m_v,m_h} e^{-j(\theta_{m_v,m_h} - m_v\xi_1 - m_h\zeta_1)} \\ &= \beta_{m_v,m_h} e^{-j(\theta_{m_v,m_h} - \tau(\Omega_1)\mathbf{m})}. \end{aligned} \quad (22)$$

We note that $\boldsymbol{\lambda}$ depends on the AoA of the incident beams at the RIS, i.e., Ω_1, as well as the RIS parameters $\boldsymbol{\Theta}$. Using equations *(5)* and *(8)*, we can restate the reference gain of the RIS in direction $\psi = [\xi, \zeta]$ by explicitly defining $G(\xi, \zeta, \boldsymbol{\lambda})$ as follows

$$G(\xi, \zeta, \boldsymbol{\lambda}) = \left|\left(\mathbf{d}_{M_v}(\xi) \otimes \mathbf{d}_{M_h}(\zeta)\right)^H \boldsymbol{\lambda}\right|^2. \quad (23)$$

On the other hand, the gain of UPA-antenna and the feed coefficients $\mathbf{c}$ is given by

$$G(\xi, \zeta, \mathbf{c}) = \left|\left(\mathbf{d}_{M_v}(\xi) \otimes \mathbf{d}_{M_h}(\zeta)\right)^H \mathbf{c}\right|^2 \quad (24)$$

that has a clear similarity.

This means that to design the RIS-UPA for the STMR problem with receive zone $\mathcal{D}$ we can use the multi-beamforming design framework to cover the ACIs included in $\mathcal{D}$ for the UPA-antenna [29]. In particular, an RIS-UPA with parameters $\boldsymbol{\lambda}$ and a UPA-antenna with beam-forming parameters $\mathbf{c}$ have the same beam-forming gain pattern if UPA structures are the same and $\boldsymbol{\lambda} = \mathbf{c}$. Hence, an RIS-UPA which is excited from the solid angle Ω_1 has the same beam-forming gain as its UPA-antenna counterpart if $\boldsymbol{\Theta} = \text{diag}\{\mathbf{c}^T \odot \mathbf{a}_M^H(\Omega_1)\}$. In the following, we address the design of beam-forming coefficients of $\mathbf{c}$ for an antenna with UPA structure which can then be used to design a RIS-UPA.

For any normalized beam-forming vector $\mathbf{c}$, it is straightforward to show that

$$\int_{-\pi}^{\pi}\int_{-\pi}^{\pi} G(\xi, \zeta, \mathbf{c})\, d\xi d\zeta = (2\pi)^2 \quad (25)$$

that can be interpreted as the power conservation law [34]. Please note that the dependence between variables ξ and ζ can be resolved using the approximation in [35]. The power conservation law *(25)* allows us to define an optimization problem for the UPA multi-beamforming design in terms of a normalized gain pattern where the total gain is divided by $(2\pi)^2$.

In the next section, we define the multi-beamforming design problem as the core of designing our proposed RIS structure.

4.4 Multi-beamforming design problem formulation

We wish to design beam-formers that provide high, sharp, and constant gain within the desired ACIs and zero gain everywhere else. We have then for the ideal gain corresponding to such beam-former $\mathbf{c}$ that,

$$\begin{aligned}\iint_{\mathcal{B}^\psi} G_{\mathcal{D}}^{\text{ideal}}(\xi, \zeta) d\xi d\zeta &= \sum_{i=1}^{k} \iint_{\mathcal{D}_i} t d\xi d\zeta \\ = \sum_{(p,q)\in\mathcal{A}} \iint_{\mathcal{B}^\psi_{p,q}} t d\xi d\zeta &= \sum_{(p,q)\in\mathcal{A}} \delta_{p,q} t = (2\pi)^2 \end{aligned} \quad (26)$$

where $\delta_{p,q} = \delta_v\delta_h$ denotes the area of the (p, q)-th beam in the (ξ, ζ) domain. Therefore, we can derive $t = \frac{(2\pi)^2}{|\mathcal{A}|\delta_{p,q}}$. It holds that,

$$G_{\mathcal{D}}^{\text{ideal}}(\xi, \zeta) = \frac{(2\pi)^2}{|\mathcal{A}|\delta_{p,q}} 1_{\mathcal{D}}(\xi, \zeta) \quad (27)$$

Using the beam-former $\mathbf{c}$ we wish to mimic the deal gain in equation *(27)*. Therefore, we formulate the following optimization problem,

$$\mathbf{c}_{\mathcal{D}}^{opt}=\underset{\mathbf{c},\|\mathbf{c}\|=1}{\arg\min}\iint_{\mathcal{B}^{\psi}}\left|G_{\mathcal{D}}^{\text{ideal}}\left(\xi,\zeta\right)-G\left(\xi,\zeta,\mathbf{c}\right)\right|d\xi d\zeta \quad (28)$$

By partitioning the range of (ξ,ζ) into predefined intervals and then uniformly sampling with the rate (L_v,L_h) per interval along both axis, we can rewrite the optimization problem as follows,

$$\begin{aligned}\mathbf{c}_{\mathcal{D}}^{opt}&=\arg\min\nolimits_{\mathbf{c},\|\mathbf{c}\|=1}\\&\sum_{r=1}^{Q_v}\sum_{s=1}^{Q_h}\iint_{\mathcal{B}^{\psi}_{r,s}}\left|G_{\mathcal{D}}^{\text{ideal}}\left(\xi,\zeta\right)-G\left(\xi,\zeta,\mathbf{c}\right)\right|d\xi d\zeta\\&=\lim_{L_h,L_v\to\infty}\sum_{r=1}^{Q_v}\sum_{s=1}^{Q_h}\sum_{l_v=1}^{L_v}\sum_{l_h=1}^{L_h}\frac{\delta_v\delta_h}{L_hL_v}\\&\left|G_{\mathcal{D}}^{\text{ideal}}\left(\xi_{r,l_v},\zeta_{s,l_h}\right)-G\left(\xi_{r,l_v},\zeta_{s,l_h},\mathbf{c}\right)\right| \quad (29)\end{aligned}$$

where,

$$\xi_{r,l_v}=\xi^{r-1}+l_v\frac{\delta_v}{L_v},\quad \zeta_{s,l_h}=\zeta^{s-1}+l_h\frac{\delta_h}{L_h} \quad (30)$$

We can rewrite equation *(29)* as,

$$\mathbf{c}_{\mathcal{D}}^{opt}=\arg\min_{\mathbf{c},\|\mathbf{c}\|=1}\lim_{L_h,L_v\to\infty}\frac{1}{L_hL_v}\left|\mathbf{G}_{\mathcal{D}}^{\text{ideal}}-\mathbf{G}(\mathbf{c})\right| \quad (31)$$

where,

$$\mathbf{G}(\mathbf{c})=\delta_{p,q}\left[G\left(\xi_{1,1},\zeta_{1,1},\mathbf{c}\right)\cdots G\left(\xi_{Q_v,L_v},\zeta_{Q_h,L_h},\mathbf{c}\right)\right]^T \quad (32)$$

and,

$$\mathbf{G}_{\mathcal{D}}^{\text{ideal}}=\delta_{p,q}\left[G_{\mathcal{D}}^{\text{ideal}}\left(\xi_{1,1},\zeta_{1,1}\right)\cdots G_{\mathcal{D}}^{\text{ideal}}\left(\xi_{Q_v,L_v},\zeta_{Q_h,L_h}\right)\right]^T \quad (33)$$

Unfortunately, the optimization problem in *(31)* does not admit an optimal closed-form solution as is, due to the absolute values of the complex numbers existing in the formulation. However, note that,

$$\begin{aligned}\mathbf{G}_{\mathcal{D}}^{\text{ideal}}&=\sum_{(p,q)\in\mathcal{A}}\delta_{p,q}\frac{(2\pi)^2}{|\mathcal{A}|\delta_{p,q}}\left(\mathbf{e}_{p,q}\otimes\mathbf{1}_{L,1}\right)\\&=\frac{(2\pi)^2}{|\mathcal{A}|}\sum_{(p,q)\in\mathcal{A}}\mathbf{e}_{p,q}\otimes\mathbf{1}_{L,1} \quad (34)\end{aligned}$$

with $\mathbf{e}_{p,q}\in\mathbb{Z}^Q$ being the standard basis vector for the (p,q)-th axis among (Q_v,Q_h) pairs. Now, note that $\mathbf{1}_{L,1}=\mathbf{g}\odot\mathbf{g}^*$ for any equal gain $\mathbf{g}\in\mathbb{C}^L$ where $L=L_hL_v$. An equal-gain vector $\mathbf{g}\in\mathbb{C}^L$ is a vector where all elements have equal absolute values (in this case, equal to 1). Therefore, we can write:

$$\begin{aligned}\mathbf{G}_{\mathcal{D}}^{\text{ideal}}&=\sum_{(p,q)\in\mathcal{A}}\frac{(2\pi)^2}{|\mathcal{A}|}\left(\mathbf{e}_{p,q}\otimes(\mathbf{g}\odot\mathbf{g}^*)\right)\\&=\frac{(2\pi)^2}{|\mathcal{A}|}\sum_{(p,q)\in\mathcal{A}}\left(\mathbf{e}_{p,q}\otimes\mathbf{g}\right)\odot\left(\mathbf{e}_{p,q}\otimes\mathbf{g}\right)^*\\&=\left(\sum_{(p,q)\in\mathcal{A}}\frac{2\pi}{\sqrt{|\mathcal{A}|}}\left(\mathbf{e}_{p,q}\otimes\mathbf{g}\right)\right)\\&\odot\left(\sum_{(p,q)\in\mathcal{A}}\frac{2\pi}{\sqrt{|\mathcal{A}|}}\left(\mathbf{e}_{p,q}\otimes\mathbf{g}\right)\right)^* \quad (35)\end{aligned}$$

Also, it is straightforward to write,

$$\mathbf{G}(\mathbf{c})=\left(\mathbf{D}^H\mathbf{c}\right)\odot\left(\mathbf{D}^H\mathbf{c}\right)^* \quad (36)$$

where, $\mathbf{D}^H=\sqrt{\delta_v\delta_h}(\mathbf{D}_v^H\otimes\mathbf{D}_h^H)$, and for $a\in\{v,h\}$, and $b\in[Q_a]$ we have,

$$\mathbf{D}_a=\left[\mathbf{D}_{a,1},\cdots,\mathbf{D}_{a,Q_a}\right]\in\mathbb{C}^{M_a\times L_aQ_a} \quad (37)$$

where,

$$\mathbf{D}_{v,b}=\left[\mathbf{d}_{M_v}\left(\xi_{b,1}\right),\cdots,\mathbf{d}_{M_v}\left(\xi_{b,L_v}\right)\right]\in\mathbb{C}^{M_v\times L_v} \quad (38)$$

$$\mathbf{D}_{h,b}=\left[\mathbf{d}_{M_h}\left(\zeta_{b,1}\right),\cdots,\mathbf{d}_{M_h}\left(\zeta_{b,L_h}\right)\right]\in\mathbb{C}^{M_h\times L_h} \quad (39)$$

Comparing the expressions *(31)*, *(35)*, and *(36)*, one can show that the optimal choice of $\mathbf{c}_{\mathcal{D}}$ in *(28)* is the solution to the following optimization problem for proper choices of $\mathbf{g}_{p,q}$.

Problem 1. *Given equal-gain vectors* $\mathbf{g}_{p,q}\in\mathbb{C}^L$, *for* $(p,q)\in\mathcal{A}$ *find vector* $\mathbf{c}_{\mathcal{D}}\in\mathbb{C}^M$ *such that*

$$\mathbf{c}_{\mathcal{D}}=\underset{\mathbf{c},\|c\|=1}{\arg\min}\lim_{L\to\infty}\left\|\sum_{(p,q)\in\mathcal{A}}\frac{2\pi}{\sqrt{|\mathcal{A}|}}\left(\mathbf{e}_{p,q}\otimes\mathbf{g}_{p,q}\right)-\mathbf{D}^H\mathbf{c}\right\|^2 \quad (40)$$

However, we now need to find the optimal choices of $\mathbf{g}_{p,q}$ that minimize the objective in *(31)*. Using *(35)* and *(36)*, we have the following optimization problem.

Problem 2. *Find equal-gain vectors* $\mathbf{g}^*_{p,q}\in\mathbb{C}^L$, $(p,q)\in\mathcal{A}$ *such that*

$$\begin{aligned}&<\mathbf{g}^*_{p,q}>_{(p,q)\in\mathcal{A}}=\underset{<\mathbf{g}_{p,q}>_{(p,q)\in\mathcal{A}}}{\arg\min}\\&\left\|abs(\mathbf{D}^H\mathbf{c}_{\mathcal{D}})-\frac{2\pi}{\sqrt{|\mathcal{A}|}}abs(\sum_{(p,q)\in\mathcal{A}}\mathbf{e}_{p,q}\otimes\mathbf{g}_{p,q})\right\|^2 \quad (41)\end{aligned}$$

where $abs(.)$ *denotes the element-wise absolute value of a vector.*

In the next section we continue with the solution of problems 1 and 2.

5. PROPOSED MULTI-BEAMFORMING DESIGN SOLUTION

Note that the solution to Problem 1 is the limit of the sequence of solutions to a least-square optimization problem as L goes to infinity. For each L we find that,

$$\mathbf{c}_{\mathcal{D}}^{(L)} = \sum_{(p,q)\in\mathcal{A}} \frac{2\pi}{\sqrt{|\mathcal{A}|}} (\mathbf{D}\mathbf{D}^H)^{-1}\mathbf{D}\left(\mathbf{e}_{p,q}\otimes\mathbf{g}_{p,q}\right) \quad (42)$$

$$\mathbf{c}_{\mathcal{D}}^{(L)} = \sum_{(p,q)\in\mathcal{A}} \sigma(\mathbf{D}_{v,p}\otimes\mathbf{D}_{h,q})\mathbf{g}_{p,q} \quad (43)$$

where $\sigma = \frac{2\pi\sqrt{\delta_v\delta_h}}{LQ\delta_v\delta_h\sqrt{|\mathcal{A}|}} = \frac{2\pi}{LQ\sqrt{\delta_v\delta_h|\mathcal{A}|}}$, noting that it holds that,

$$\mathbf{D}\mathbf{D}^H = \delta_v\delta_h(\mathbf{D}_v\otimes\mathbf{D}_h)(\mathbf{D}_v^H\otimes\mathbf{D}_h^H) = \delta_v\delta_h LQ \doteq \kappa \quad (44)$$

Even though Problem 1 admits a nice analytical closed form solution, doing so for the Problem 2 is not a trivial task, especially due to the fact that the objective function is not convex. However, the convexification of the objective problem in the form of

$$\begin{aligned} &< \mathbf{g}_{p,q}^* >_{(p,q)\in\mathcal{A}} \\ &= \underset{<\mathbf{g}_{p,q}>_{(p,q)\in\mathcal{A}}}{\arg\min} \left\| \mathbf{D}^H\mathbf{c}_{\mathcal{D}} - \frac{2\pi}{\sqrt{|\mathcal{A}|}} \sum_{(p,q)\in\mathcal{A}} \mathbf{e}_{p,q}\otimes\mathbf{g}_{p,q} \right\|^2 \\ &= \underset{<\mathbf{g}_{p,q}>_{(p,q)\in\mathcal{A}}}{\arg\min} \left\| \left(\kappa\mathbf{D}^H\mathbf{D} - \mathbf{I}_{LQ}\right) \sum_{(p,q)\in\mathcal{A}} \mathbf{e}_{p,q}\otimes\mathbf{g}_{p,q} \right\|^2 \end{aligned} \quad (45)$$

leads to an effective solution for the original problem. Indeed, it can be verified by solving the optimization problem *(45)* numerically that the solution admits the form *(46)* in the following conjecture.

Conjecture 3. *The minimizer of (45) is in the form of*

$$\mathbf{g}_{p,q}^* = \begin{bmatrix} 1 & \alpha_v\alpha_h & \cdots & \alpha_v^{(L_v-1)}\alpha_h^{(L_h-1)} \end{bmatrix}^T, (p,q)\in\mathcal{A} \quad (46)$$

for some η_v, η_h where $\alpha_a = e^{j(\frac{\eta_a}{L_a})}$, $a\in\{v,h\}$.

Except for some special cases, we have not been able to analytically prove this conjecture in its entirety. In the following, we use the the analytical form *(46)* for $\mathbf{g}_{p,q}^*$ for the rest of our derivations. This solution would not be the optimal solution for the original problem *(41)*. However, it provides a near-optimal solution with added benefits of allowing us to (i) find the limit of the solution as L goes to infinity, and (ii) express the beam-forming vectors in closed form, as it will be revealed in the following discussion. An analytical closed form solution for $\mathbf{c}_{\mathcal{D}}$ can be found as follows. It holds that,

$$\begin{aligned} \mathbf{c}_{\mathcal{D}}^{(L)} &= \sum_{(p,q)\in\mathcal{A}} \left(\sum_{(l_v,l_h)=(1,1)}^{(L_v,L_h)} \sigma g_{p,q,l_v,l_h} \mathbf{d}_{M_t}\left(\xi_{p,l_v},\zeta_{q,l_h}\right) \right) \\ &= \sum_{(p,q)\in\mathcal{A}} \\ &\left(\sum_{(l_v,l_h)=(1,1)}^{(L_v,L_h)} \sigma g_{q,p,l_v,l_h} \left[1,\cdots,e^{j\mu_{p,q,l_v,l_h}^{M_v-1,M_h-1}}\right]^T \right) \end{aligned} \quad (47)$$

where $\mu_{p,q,l_v,l_h}^{m_v,m_h} = (m_v\xi_{p,l_v} + m_h\zeta_{q,l_h})$. We can then write for the $(m_v,m_h)^{th}$ component of the beam-former $\mathbf{c}_{\mathcal{D}}$,

$$\begin{aligned} c_{p,q,m_v,m_h} &= \lim_{L_h,L_v\to\infty} \frac{1}{L_hL_v} \\ &\sum_{(p,q)\in\mathcal{A}} \sum_{(l_h,l_v)=(1,1)}^{(L_h,L_v)} g_{p,q,l_v,l_h} e^{j\mu_{p,q,l_v,l_h}^{M_v-1,M_h-1}} \end{aligned} \quad (48)$$

Using equation *(30)*, we can rewrite *(48)* as,

$$\begin{aligned} c_{p,q,m_v,m_h} =& \frac{2\pi}{Q} e^{j\chi_{p-1,q-1}^{m_v,m_h}} \left(\frac{1}{L_v} \lim_{L_v\to\infty} \sum_{l_v=1}^{L_v} e^{j\frac{\eta_v+m_v\delta_v}{L_v}l_v} \right) \\ &\left(\frac{1}{L_h} \lim_{L_h\to\infty} \sum_{l_h=1}^{L_h} e^{j\frac{\eta_h+m_h\delta_h}{L_h}l_h} \right) \end{aligned} \quad (49)$$

to get,

$$\begin{aligned} &c_{\mathcal{D},m_v,m_h} \\ &= \sum_{(p,q)\in\mathcal{A}} \frac{2\pi}{Q} e^{j\chi_{p-1,q-1}^{m_v,m_h}} \int_0^1 e^{j\xi_v x}dx \int_0^1 e^{j\xi_h x}dx \\ &= \sum_{(p,q)\in\mathcal{A}} \frac{2\pi}{Q} e^{j(\zeta_{p-1,q-1}^{m_v,m_h} + \frac{\xi_v+\xi_h}{2})} sinc(\frac{\xi_v}{2\pi}) sinc(\frac{\xi_h}{2\pi}) \end{aligned} \quad (50)$$

with $\chi_{p,q}^{m_v,m_h} = (m_v\xi^p + m_h\zeta^q)$, and $\xi_a = \delta_a m_a + \eta_a$, for $a\in\{v,h\}$. Now that the closed-form expression for $\mathbf{c}_{\mathcal{D}}$, and therefore, $\boldsymbol{\lambda}$ is known, for an RIS that is excited from the solid angle Ω_1, the RIS parameters at the antenna placed at location (m_v,m_h) can be easily computed. More precisely, we get,

$$\beta_{m_v,m_h} = |\mathbf{c}_{\mathcal{D},m_v,m_h}| \quad (51)$$

$$\theta_{m_v,m_h} = \underline{/\mathbf{c}_{\mathcal{D},m_v,m_h}} + m_v\xi_1 + m_h\zeta_1 \quad (52)$$

The solution given by *(51)* and *(52)* is optimized to find a beam-forming pattern which is the closest to the desired normalized beam pattern. However, in practice the norm of **c** depends on the power P that can be inserted by amplifiers (active elements), say $\|\mathbf{c}\| \leq P$. Hence for an RIS-UPA with active elements the gains β_{m_v,m_h} is scaled by $\sqrt{P}$. Also, the solution given by *(51)* and *(52)* may be further tailored for the case that the RIS elements are passive.

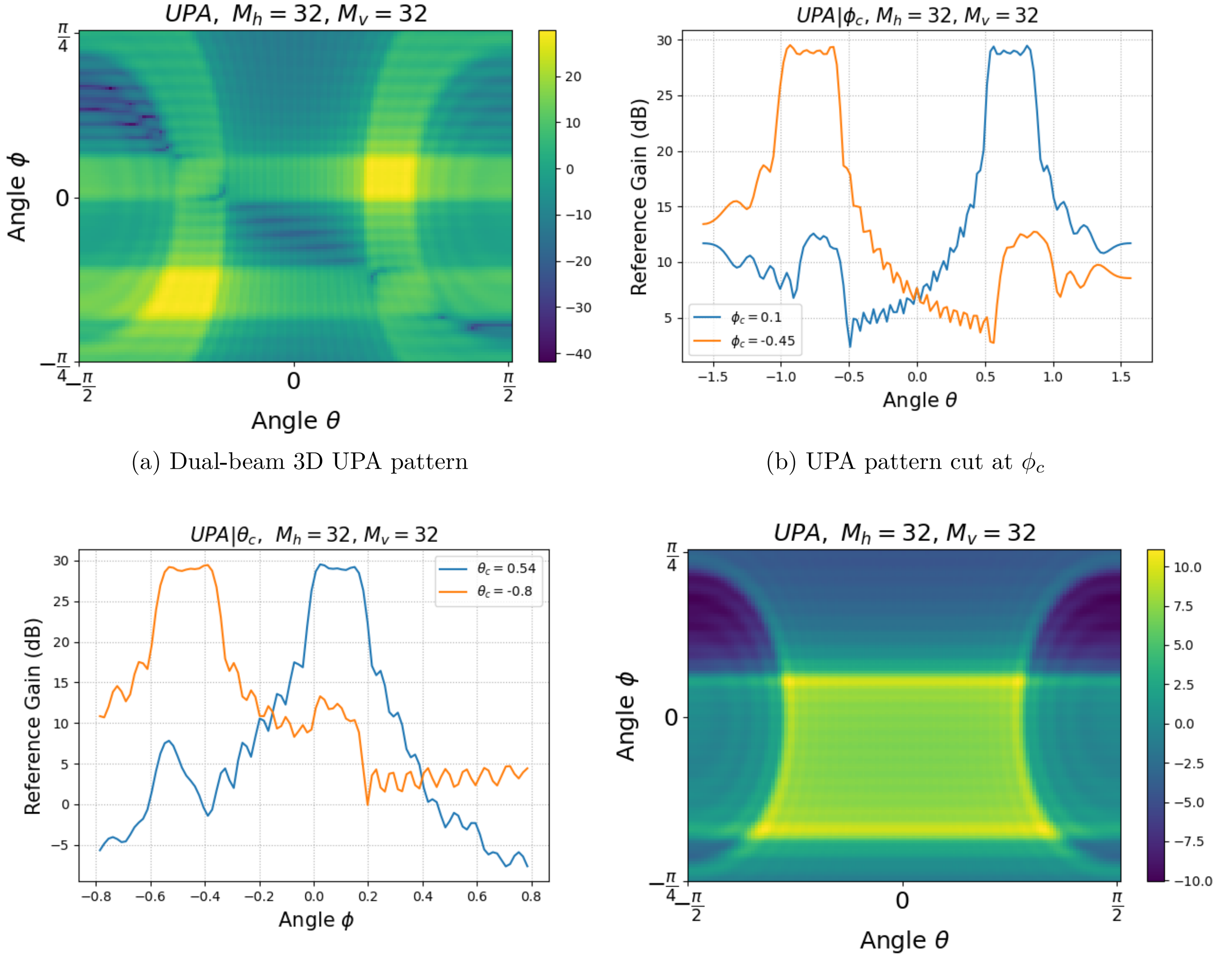

(a) Dual-beam 3D UPA pattern

(b) UPA pattern cut at ϕ_c

(c) UPA pattern cut at θ_c

(d) 3D UPA pattern

Fig. 4 – RIS-UPA beam patterns for multi-beamforming settings

If the gain control for the passive RIS elements is still possible, the absolute value of the gain for each element may not exceed 1 (a value less than 1 corresponds to an attenuation). In order to maximize the power reflected by the RIS, we scale the gains β_{m_v,m_h} so that their maximum is equal to one, i.e., $\beta_{m_v,m_h} = |\mathbf{c}_{\mathcal{D},m_v,m_h}|/\|\mathbf{c}\|_\infty$. Finally, in the case that gain control (attenuation) at the RIS with passive elements is not feasible, we have $\beta_{m_v,m_h} = 1$. In the next section, we evaluate the effectiveness of our RIS beam-forming design approach by means of numerical experiments.

6. PERFORMANCE EVALUATION

In this section, we evaluate the performance of our multi-beam design framework.

6.1 Multibeam design

First, we consider a dual-beam design which comprises of two lobes with centers at directions $(-8\pi/32, -5\pi/32)$ and $(7\pi/32, \pi/32)$ for the pairs of the solid angle (ϕ, θ) with the beamwidth equal to $\pi/16$. We divide both the ψ_h, and the ψ_v range uniformly into $Q_h = 16$, and $Q_v = 16$ regions resulting in $Q = 256$ equally-shaped units in (ψ_v, ψ_h) domain. We cover each desired beam with the smallest number of the designed units to provide uniform gain at the desired angular regions. Figures 4(a)-(c) depict the beam pattern of the dual beam obtained through our design where all angles are measured in radians. Fig. 4(a) shows the heat map corresponding to the gain of the reflected beam from the RIS for the designed dual-beam. The gains are computed in dB. It can be seen that the designed beam-former generates two disjoint beams with an almost uniform gain over the desired ACIs. It is also observed that the beams sharply drop outside

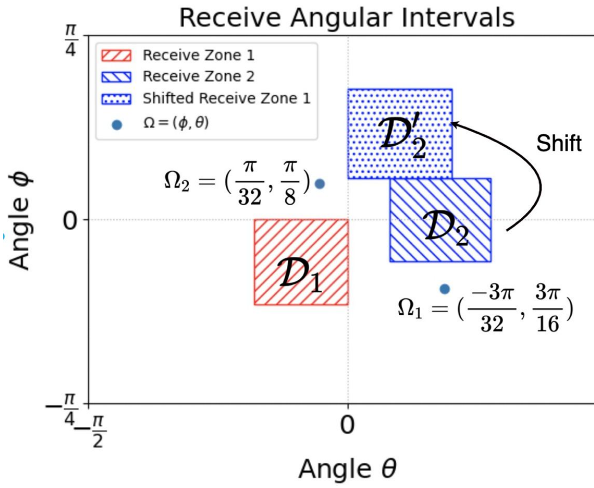

(a) Receive angular intervals

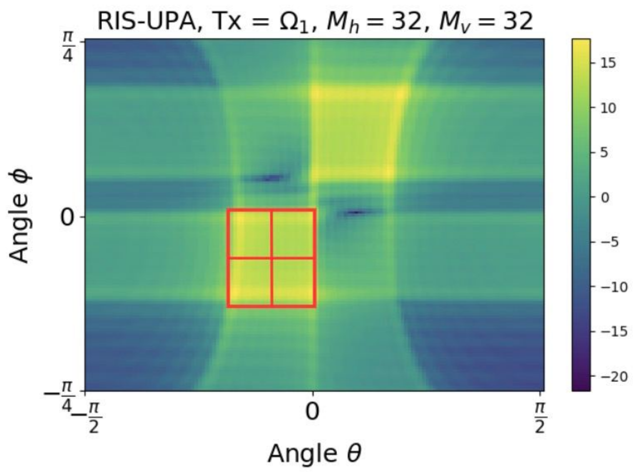

(b) RIS pattern at incident angle Ω_1

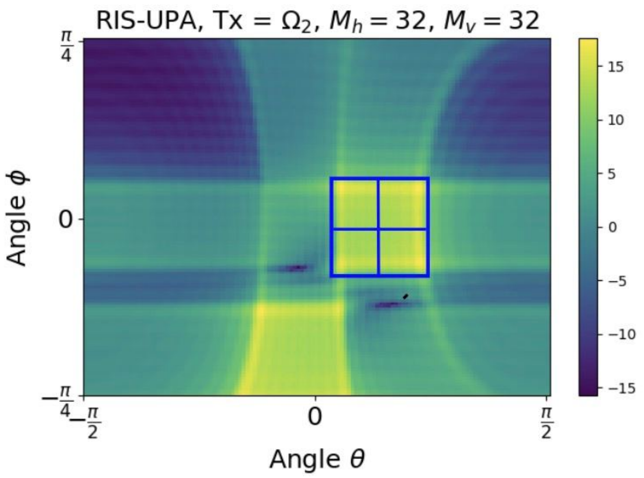

(c) RIS pattern at incident angle Ω_2

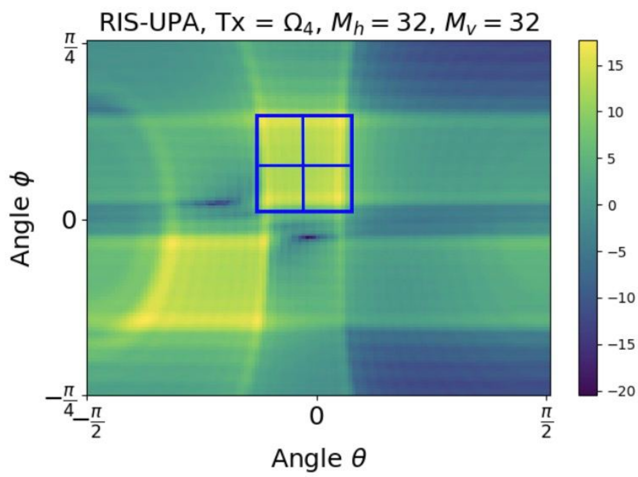

(d) RIS pattern at incident angle Ω_4

Fig. 5 – RIS-UPA beam patterns for MTMR settings

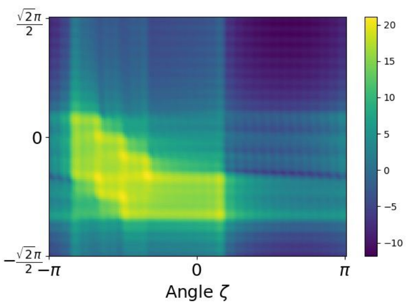

(a) $(Q_h, Q_v) = (12, 12)$

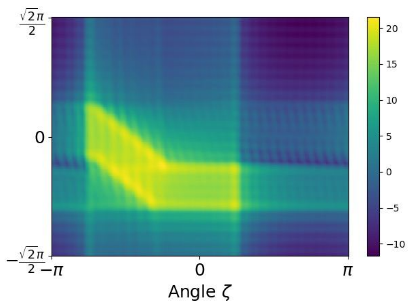

(b) $(Q_h, Q_v) = (24, 24)$

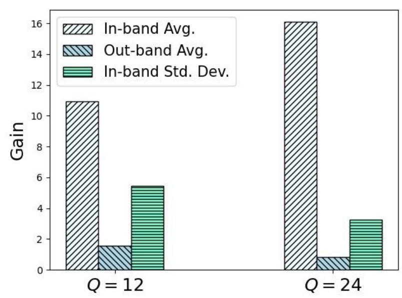

(c) Beam pattern statistics

Fig. 6 – Effect of resolution on the beam quality

the desired ACIs and effectively suppress the gain everywhere outside the ACI. In order to quantify the suppression and the leakage out of the desired ACI we depict the cross-section of the gain pattern at a fixed elevation angle ϕ_c for two values of $\phi_c \in \{-8\pi/32, 7\pi/32\}$ located inside the two lobes of the designed dual beam in Fig. 4(b). Similarly, Fig. 4(c) shows the cross-section of the beam pattern at a fixed azimuth angle θ_c for two values of $\theta_c \in \{-5\pi/32, \pi/32)\}$. Both Fig. 4(b) and Fig. 4(c) confirm the sharpness of both lobes of the designed dual-beam and can be used to find the beamwidth of each lobes at an arbitrary fraction from its maximum values, e.g., the 3dB beamwidth or 10dB beamwidth. Indeed, there is a negligible difference between 3dB and 10dB beamwidth which clarifies the sharpness of the beams. From Fig. 4(b) and Fig. 4(c), it is also observed that the gain within the ACI is almost uniform. Nonetheless, we should emphasize the fact that the shape of the lobes of the beam that are centered at different solid angles may suffer from slight deformation as seen by Fig. 4(a). This phenomenon worsens as the corresponding lobes of the beams get too close to the plane of the RIS.

6.2 Comparison of multibeam and single beam

In order to compare the performance of our multi beam design to a single-beam design, we consider a beam with a single lobe which is capable of covering the same two regions as in the dual-beam design. Fig. 4(d) shows the heat map corresponding to the gain of the reflected beam from an RIS for the corresponding single beam that is optimized based on our design. As was the case for multibeam, this figure also shows that for a single beam our design generates an almost uniform and fairly sharp beam. However, comparing Fig. 4(a) and Fig. 4(d), we observe that in the desired ACI the multi-beamforming procedure enhances the gain by about 20 dB over the beams with an optimized single lobe. The reason for this difference is that according to the power conservation axiom, with a constant input power level, the narrower each beam is the higher will be the reference gain over the area it covers. In fact, if we target two disjoint ACIs with a single beam, the beam must be wide enough to cover both areas. This will result in dissipating the power in angles that are not intended. However, the muti-beam design allows for generating two disjoint beams, each being narrow enough to only cover the intended ACI. Therefore, the power will not be wasted in undesired directions.

6.3 Two-way multi-link communications

We consider two links. The first link is between the transmitter located as $\Omega_1 = (\frac{-3\pi}{32}, \frac{3\pi}{16})$ and a receiver that is in the ACI $\mathcal{D}_1 = [-0.36, 0] \times [-0.56, 0]$ and the second link is between the transmitter located as $\Omega_2 = (\frac{\pi}{32}, \frac{\pi}{8})$ and a receiver that is in the ACI $\mathcal{D}_1 = [-0.18, 0.18] \times [0.26, 0.86]$. Each of the receive zones $\mathcal{D}_1$ and $\mathcal{D}_2$ is comprised of 4 particles in an $Q_v \times Q_h = 8 \times 8$ grid. Fig. 5(a) depicts the angular location of the two transmitters and the ACI for the receivers. In order to design a beam-former that covers $\mathcal{D}_1$ when transmitting from angular position Ω_1 and covers $\mathcal{D}_2$ when transmitting from angular position Ω_2, we first find a composite beam with a unified incident angle, say Ω_1. This means that we find the ACI $\mathcal{D}_2'$ when the RIS array is excited by a beam at incident angle Ω_1 which is equivalent to the ACI $\mathcal{D}_2$ where the same array is excited from the incident angle Ω_2. The transformed ACI $\mathcal{D}_2'$ is depicted in Fig 5(a). The heat map of the designed beams is depicted in figures 5(b)-(d) where the RIS is excited from angles Ω_1, Ω_2, and Ω_4, respectively. Figures 5(b)-(c) illustrate that when the RIS is excited from an incident angle Ω_1 and Ω_2, the corresponding ACI $\mathcal{D}_1$ and $\mathcal{D}_2$ are respectively covered by the designed beam as illustrated in the respective figures, however, in either case another angular region is also covered by the beam which is not necessary and could be considered as possible wastage of the power. We note that this happens due to the fact that the unwanted ACI when the RIS is excited from the incident angle Ω_1 is indeed generating the desired ACI when the RIS is excited from the incident angle Ω_2. Finally, we consider Ω_4 to be an angular point in the ACI $\mathcal{D}_2$, e.g., we take Ω_4 to be the center of the ACI $\mathcal{D}_2$. Fig. 5(d) shows that if the RIS is excited from an incident angle Ω_4, e.g., when a user in ACI $\mathcal{D}_2$ is replying, then it will be received by the corresponding transmitter which is located at angular position Ω_2. In figures 5(b)-(d) the windows show the positioning of the grids that lie on the particles covering the corresponding desired ACIs.

6.4 Beams with arbitrary shape (footprint)

Here, we illustrate the possibility of designing a beam with an arbitrary pattern, or more precisely, arbitrary footprint. We aim to design a beam which is covering the receive zone $\mathcal{D}$ that is specified as follows.

$$\mathcal{D} = \begin{cases} -\frac{\sqrt{2}}{2}(\zeta + \frac{11}{6}) < \xi < -\frac{\sqrt{2}}{2}(\zeta + \frac{3}{2}) & \text{if } \frac{-5\pi}{6} \leq \zeta \leq \frac{-\pi}{3} \\ \frac{-7\sqrt{2}\pi}{24} < \xi < \frac{-3\sqrt{2}\pi}{24} & \text{if } \frac{-\pi}{3} < \zeta \leq \frac{\pi}{3} \end{cases} \tag{53}$$

We consider two possible quantization levels of the beam footprint with resolution $Q_h = Q_v = 12$ and $Q_h = Q_v = 24$. Fig. 6(a) and Fig. 6(b) illustrate the heat map of the designed beam. The finer the resolution the better the approximation of the shape of the beam. Fig. 6(c) provides the quantitative comparison between these two resolutions; it shows the higher resolution increases the overall beam-forming gain, lowers the leakage and generates smoother gain.

7. CONCLUSIONS

An RIS can be incorporated into mmWave communications to fill the coverage gaps in the blind spots of the mmWave system. We proposed a novel approach for designing RISs, namely RIS-UPA, where the RIS elements are arranged according to a UPA structure. We proposed a configuration for the elements of an RIS-UPA that enables the coverage of multiple disjoint angular intervals simultaneously. On this ground, we showed that an RIS-UPA assisted MIMO system can support multiple two-way communication pairs simultaneously.

We established that the RIS-aided multiple-pair scenario can be transformed to a single-pair scenario and then by appealing to the similarities of RIS-UPA and UPA beamforming we argued that we can borrow the principles of UPA multi-beamforming design to obtain closed-form low-complexity solutions for the RIS design problem. Both our theoretical results and numerical experiments demonstrate that our RIS configuration can form beams of custom footprints and will result in sharp, high, and stable gains within the desired ACIs regardless of their spatial locations, while effectively suppressing all the undesired out-of-band components.

REFERENCES

[1] Chongwen Huang, Alessio Zappone, George C. Alexandropoulos, Mérouane Debbah, and Chau Yuen. "Reconfigurable Intelligent Surfaces for Energy Efficiency in Wireless Communication". In: *IEEE Transactions on Wireless Communications* 18.8 (2019), pp. 4157–4170. DOI: 10.1109/TWC.2019.2922609.

[2] Christos Liaskos, Shuai Nie, Ageliki Tsioliaridou, Andreas Pitsillides, Sotiris Ioannidis, and Ian Akyildiz. "A New Wireless Communication Paradigm through Software-Controlled Metasurfaces". In: *IEEE Communications Magazine* 56.9 (2018), pp. 162–169. DOI: 10.1109/MCOM.2018.1700659.

[3] Ertugrul Basar, Marco Di Renzo, Julien De Rosny, Merouane Debbah, Mohamed-Slim Alouini, and Rui Zhang. "Wireless Communications Through Reconfigurable Intelligent Surfaces". In: *IEEE Access* 7 (2019), pp. 116753–116773. DOI: 10.1109/ACCESS.2019.2935192.

[4] Chen Hu, Linglong Dai, Shuangfeng Han, and Xiaoyun Wang. "Two-Timescale Channel Estimation for Reconfigurable Intelligent Surface Aided Wireless Communications". In: *IEEE Transactions on Communications* (2021), pp. 1–1. DOI: 10.1109/TCOMM.2021.3072729.

[5] Ertugrul Basar. "Reconfigurable Intelligent Surface-Based Index Modulation: A New Beyond MIMO Paradigm for 6G". In: *IEEE Transactions on Communications* 68.5 (2020), pp. 3187–3196. DOI: 10.1109/TCOMM.2020.2971486.

[6] Zhaohui Yang, Wei Xu, Chongwen Huang, Jianfeng Shi, and Mohammad Shikh-Bahaei. "Beamforming Design for Multiuser Transmission Through Reconfigurable Intelligent Surface". In: *IEEE Transactions on Communications* 69.1 (2021), pp. 589–601. DOI: 10.1109/TCOMM.2020.3028309.

[7] Xiaojun Yuan, Ying-Jun Angela Zhang, Yuanming Shi, Wenjing Yan, and Hang Liu. "Reconfigurable-Intelligent-Surface Empowered Wireless Communications: Challenges and Opportunities". In: *IEEE Wireless Communications* 28.2 (2021), pp. 136-143 DOI: 10.1109/MWC.001.2000256.

[8] Wankai Tang, Jun Yan Dai, Ming Zheng Chen, Kai-Kit Wong, Xiao Li, Xinsheng Zhao, Shi Jin, Qiang Cheng, and Tie Jun Cui. "MIMO Transmission Through Reconfigurable Intelligent Surface: System Design, Analysis, and Implementation". In: *IEEE Journal on Selected Areas in Communications* 38.11 (2020), pp. 2683–2699. DOI: 10.1109/JSAC.2020.3007055.

[9] Chongwen Huang, Ronghong Mo, and Chau Yuen. "Reconfigurable Intelligent Surface Assisted Multiuser MISO Systems Exploiting Deep Reinforcement Learning". In: *IEEE Journal on Selected Areas in Communications* 38.8 (2020), pp. 1839–1850. DOI: 10.1109/JSAC.2020.3000835.

[10] Ruiqi Liu, Qingqing Wu, Marco Di Renzo, and Yifei Yuan. *A Path to Smart Radio Environments: An Industrial Viewpoint on Reconfigurable Intelligent Surfaces*. 2021. arXiv: 2104.14985 [cs.NI].

[11] Daisuke Kitayama, Yuto Hama, Kenta Goto, Kensuke Miyachi, Takeshi Motegi, and Osamu Kagaya. "Transparent dynamic metasurface for a visually unaffected reconfigurable intelligent surface: controlling transmission/reflection and making a window into an RF lens". In: *Opt. Express* 29.18 (Aug. 2021), pp. 29292–29307. DOI: 10.1364/OE.435648. URL: http://www.opticsexpress.org/abstract.cfm?URI=oe-29-18-29292.

[12] Xilong Pei, Haifan Yin, Li Tan, Lin Cao, Zhanpeng Li, Kai Wang, Kun Zhang, and Emil Björnson. *RIS-Aided Wireless Communications: Prototyping, Adap- tive Beamforming, and Indoor/Outdoor Field Trials*. 2021. arXiv: 2103.00534 [cs.IT].

[13] Wankai Tang, Xiang Li, Jun Yan Dai, Shi Jin, Yong Zeng, Qiang Cheng, and Tie Jun Cui. "Wireless communications with programmable metasurface: Transceiver design and experimental results". In: *China Communications* 16.5 (2019), pp. 46–61. DOI: 10.23919/j.cc.2019.05.004.

[14] QurratUlAin Nadeem, Abla Kammoun, Anas Chaaban, Mérouane Debbah, and Mohamed-Slim Alouini. "Asymptotic Max-Min SINR Analysis of Reconfigurable Intelligent Surface Assisted MISO Systems". In: *IEEE Transactions on Wireless Communications* 19.12 (2020), pp. 7748–7764. DOI: 10.1109/TWC.2020.2986438.

[15] Sixian Li, Bin Duo, Xiaojun Yuan, Ying-Chang Liang, and Marco Di Renzo. "Reconfigurable Intelligent Surface Assisted UAV Communication: Joint Trajectory Design and Passive Beamforming". In: *IEEE Wireless Communications Letters* 9.5 (2020), pp. 716–720. DOI: 10.1109/LWC.2020.2966705.

[16] Anousheh Gholami, Nariman Torkzaban, John S. Baras, and Chrysa Papagianni. *Joint Mobility-Aware UAV Placement and Routing in Multi-Hop UAV Relaying Systems*. 2020. DOI: 10.48550/ARXIV.2009.14446. URL: https://arxiv.org/abs/2009.14446.

[17] Abubakar U. Makarfi, Khaled M. Rabie, Omprakash Kaiwartya, Xingwang Li, and Rupak Kharel. "Physical Layer Security in Vehicular Networks with Reconfigurable Intelligent Surfaces". In: *2020 IEEE 91st Vehicular Technology Conference (VTC2020-Spring)*. 2020, pp. 1–6. DOI: 10.1109/VTC2020-Spring48590.2020.9128438.

[18] Zahra Esmaeilbeig, Kumar Vijay Mishra, and Mojtaba Soltanalian. "IRS-Aided Radar: Enhanced Target Parameter Estimation via Intelligent Reflecting Surfaces". In: *2022 IEEE 12th Sensor Array and Multichannel Signal Processing Workshop (SAM)*. 2022, pp. 286–290. DOI: 10.1109/SAM53842.2022.9827797.

[19] Zahra Esmaeilbeig, Kumar Vijay Mishra, Arian Eamaz, and Mojtaba Soltanalian. *Cramer-Rao Lower Bound Optimization for Hidden Moving Target Sensing via Multi-IRS-Aided Radar*. 2022. DOI: 10.48550/ARXIV.2210.05812. URL: https://arxiv.org/abs/2210.05812.

[20] Yu Han, Wankai Tang, Shi Jin, Chao-Kai Wen, and Xiaoli Ma. "Large Intelligent Surface-Assisted Wireless Communication Exploiting Statistical CSI". In: *IEEE Trans. on Vehicular Tech.* 68.8 (2019), pp. 8238–8242. DOI: 10.1109/TVT.2019.2923997.

[21] Minchae Jung, Walid Saad, Youngrok Jang, Gyuyeol Kong, and Sooyong Choi. "Performance Analysis of Large Intelligent Surfaces (LISs): Asymptotic Data Rate and Channel Hardening Effects". In: *IEEE Transactions on Wireless Communications* 19.3 (2020), pp. 2052–2065. DOI: 10.1109/TWC.2019.2961990.

[22] Samith Abeywickrama, Rui Zhang, Qingqing Wu, and Chau Yuen. "Intelligent Reflecting Surface: Practical Phase Shift Model and Beamforming Optimization". In: *IEEE Trans. on Comm.* 68.9 (2020), pp. 5849–5863. DOI: 10.1109/TCOMM.2020.3001125.

[23] Huayan Guo, Ying-Chang Liang, Jie Chen, and Erik G. Larsson. "Weighted Sum-Rate Maximization for Reconfigurable Intelligent Surface Aided Wireless Networks". In: *IEEE Transactions on Wireless Communications* 19.5 (2020), pp. 3064–3076. DOI: 10.1109/TWC.2020.2970061.

[24] Boya Di, Hongliang Zhang, Lianlin Li, Lingyang Song, Yonghui Li, and Zhu Han. "Practical Hybrid Beamforming With Finite-Resolution Phase Shifters for Reconfigurable Intelligent Surface Based Multi-User Communications". In: *IEEE Transactions on Vehicular Technology* 69.4 (2020), pp. 4565–4570. DOI: 10.1109/TVT.2020.2973202.

[25] Yuanwei Liu, Xiao Liu, Xidong Mu, Tianwei Hou, Jiaqi Xu, Marco Di Renzo, and Naofal Al-Dhahir. "Reconfigurable Intelligent Surfaces: Principles and Opportunities". In: *IEEE Communications Surveys Tutorials* (2021), pp. 1–1. DOI: 10.1109/COMST.2021.3077737.

[26] Mohamed A. ElMossallamy, Hongliang Zhang, Lingyang Song, Karim G. Seddik, Zhu Han, and Geoffrey Ye Li. "Reconfigurable Intelligent Surfaces for Wireless Communications: Principles, Challenges, and Opportunities". In: *IEEE Transactions on Cognitive Communications and Networking* 6.3 (2020), pp. 990–1002. DOI: 10.1109/TCCN.2020.2992604.

[27] Saman Atapattu, Rongfei Fan, Prathapasinghe Dharmawansa, Gongpu Wang, Jamie Evans, and Theodoros A. Tsiftsis. "Reconfigurable Intelligent Surface Assisted Two–Way Communications: Performance Analysis and Optimization". In: *IEEE Transactions on Communications* 68.10 (2020), pp. 6552–6567. DOI: 10.1109/TCOMM.2020.3008402.

[28] Bei Guo, Chenhao Sun, and Meixia Tao. "Two-Way Passive Beamforming Design for RIS-Aided FDD Communication Systems". In: *2021 IEEE Wireless Communications and Networking Conference (WCNC)*. 2021, pp. 1–6. DOI: 10.1109/WCNC49053.2021.9417522.

[29] Nariman Torkzaban and Mohammad A. Amir Khojastepour. "Shaping mmWave Wireless Channel via Multi-Beam Design using Reconfigurable Intelligent Surfaces". In: *2021 IEEE Globecom Workshops (GC Wkshps)*. 2021, pp. 1–6. DOI: 10.1109/GCWkshps52748.2021.9682099.

[30] Nariman Torkzaban, Mohammad A. Amir Khojastepour, and John S. Baras. "Codebook Design for Composite Beamforming in Next-generation mmWave Systems". In: *2022 IEEE Wireless Communications and Networking Conference (WCNC)*. 2022, pp. 1545–1550. DOI: 10.1109/WCNC51071.2022.9771572.

[31] Mehrdad Nosrati, Shahram Shahsavari, Sanghoon Lee, Hua Wang, and Negar Tavassolian. "A Concurrent Dual-Beam Phased-Array Doppler Radar Using MIMO Beamforming Techniques for Short-Range Vital-Signs Monitoring". In: *IEEE Transactions on Antennas and Propagation* 67.4 (2019), pp. 2390–2404. DOI: 10.1109/TAP.2019.2893337.

[32] Jiaqi Xu, Yuanwei Liu, Xidong Mu, and Octavia A. Dobre. "STAR-RISs: Simultaneous Transmitting and Reflecting Reconfigurable Intelligent Surfaces". In: *IEEE Communications Letters* 25.9 (2021), pp. 3134–3138. DOI: 10.1109/LCOMM.2021.3082214.

[33] Yuhua Jiang, Feifei Gao, Mengnan Jian, Shun Zhang, and Wei Zhang. *Reconfigurable Intelligent Surface for Near Field Communications: Beamforming and Sensing*. 2022. DOI: 10.48550/ARXIV.2204.10114. URL: https://arxiv.org/abs/2204.10114.

[34] Sooyoung Hur, Taejoon Kim, David J. Love, James V. Krogmeier, Timothy A. Thomas, and Amitava Ghosh. "Millimeter Wave Beamforming for Wireless Backhaul and Access in Small Cell Networks". In: *IEEE Transactions on Communications* 61.10 (2013), pp. 4391–4403. DOI: 10.1109/TCOMM.2013.090513.120848.

[35] Jiho Song, Junil Choi, and David J. Love. "Common Codebook Millimeter Wave Beam Design: Designing Beams for Both Sounding and Communication With Uniform Planar Arrays". In: *IEEE Transactions on Communications* 65.4 (2017), pp. 1859–1872. DOI: 10.1109/TCOMM.2017.2665497.

AUTHORS

Nariman Torkzaban received his B.Sc. degree in electrical engineering and mathematics (minor) from Sharif University of Technology, Tehran, Iran, in 2017 and his M. S. degree from University of Maryland, College Park, MD in 2018. He is a Ph.D. candidate in the ECE department at the University of Maryland, College Park (UMD), and a member of the Institute for Systems Research (ISR). His research interests include multiuser communications, wireless networking, learning theory and its application in 5G/6G, and optimization.

Mohammad Ali (Amir) Khojastepour received a Ph.D. degree in electrical and computer engineering from Rice University, Houston, TX, USA, in 2004. Since 2004, he has been a member of the technical staff with the Mobile Communications and Networking Research Department, NEC Laboratories America Inc., Princeton, NJ, USA. His research interests include information theory and coding, communication theory, and signal processing with an emphasis on multiuser communications and wireless networks.

Mohammad Farajzadeh Tehrani received a Ph.D. degree in mathematics from Princeton University, Princeton, NJ, USA, in 2012. In 2012-2013, he was with the Department of Mathematics, in Cornell University as a visiting assistant professor. He then joined the Simons Center at Stony Brook University, as a research assistant professor until 2018. Since 2018, he has been with the Department of Mathematics at The University of Iowa as an assistant and then associate professor. His research interests lie in symplectic topology and complex algebraic geometry.

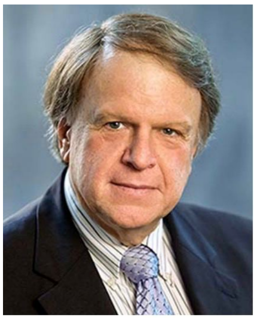

John S. Baras received a Diploma degree in electrical and mechanical engineering from the National Technical University of Athens, Athens, Greece, in 1970, and M.S. and Ph.D. degrees in applied mathematics from Harvard University, Cambridge, MA, USA, in 1971 and 1973, respectively. From 1985 to 1991, he was the founding director of the Institute for Systems Research (ISR), University of Maryland, College Park, MD, USA. He is currently a aistinguished university professor and the Lockheed Martin chair in systems engineering with the Department of Electrical and Computer Engineering, ISR. Since 1992, he has been the director of the Maryland Center for Hybrid Networks, of which he was a co-founder. His research interests include systems and control, optimization, communication networks, applied mathematics, machine learning, artificial intelligence, signal processing, robotics, computing systems, security, trust, systems biology, healthcare systems, and model-based systems engineering. Dr. Baras is a fellow of SIAM, AAAS, NAI, IFAC, AMS, and AIAA, a member of the National Academy of Inventors, and a Foreign Member of the Royal Swedish Academy of Engineering Sciences. He received the 1980 George Axelby Award from the IEEE Control Systems Society, the 2006 Leonard Abraham Prize from the IEEE Communications Society, the 2017 IEEE Simon Ramo Medal, the 2017 AACC Richard E. Bellman Control Heritage Award, and the 2018 AIAA Aerospace Communications Award. In 2018, he received the Doctorate Honoris Causa from the National Technical University of Athens, Greece. In 2016, he was inducted into the A. J. Clark School of Engineering Innovation Hall of Fame.